

THE STAR FORMATION NEWSLETTER

No. 338 27-33

2021. 4. 30 泉奈都子 (ASIAA)

27. Constraining Protoplanetary Disk Accretion and Young Planets Using ALMA Kinematic Observations

28. Accretion and outflow activity in proto-brown dwarfs

29. GASTON: Galactic Star Formation with NIKA2. Evidence for the mass growth of star-forming clumps

30. C¹⁸O, C¹³O, and C¹²O abundances and excitation temperatures in the Orion B molecular cloud: An analysis of the precision achievable when modeling spectral line within the Local Thermodynamic Equilibrium approximation

31. Dissecting the super-critical filaments embedded in the 0.5 pc subsonic region of B5

32. High-accuracy estimation of magnetic field strength in the interstellar medium from dust polarization

33. Outflows, envelopes, and disks as evolutionary indicators in Lupus YSOs

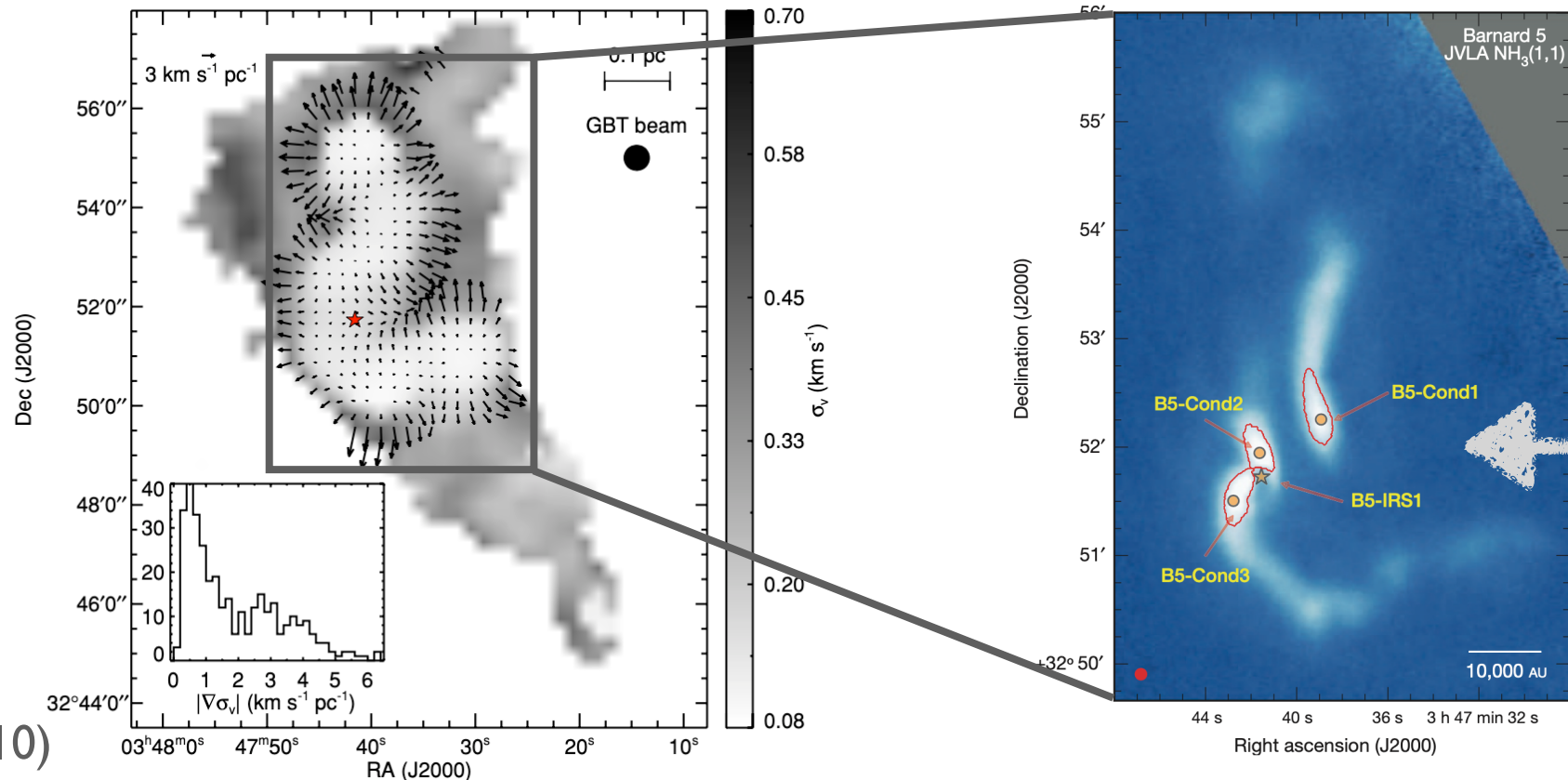
31. Dissecting the super-critical filaments embedded in the 0.5 pc subsonic region of Barnard 5

Schmiedeke et al.

<https://arxiv.org/pdf/2101.00248v1.pdf>

Subsonic region で検出されたフィラメント構造の詳細な性質を求める
(研究の目標はフィラメントの分裂過程について明らかにすること)

- Observation (Pineda et al. 2015)
 - Target: Perseus star-forming regionにあるBarnard 5 (B5)
 - $D = 302 \pm 21 \text{ kpc}$
 - Nearly constant subsonic non-thermal velocity dispersion
 - Filament structure (1 YSO, 3 gravitationally bound dense gas condensations)
→ Results of fragmentation of the dense gas filament
 - Telescope : JCMT (450, 850 μm continuum), GBT, VLA ($\text{NH}_3(1,1)$, $\text{NH}_3(2,2)$)
 - Resolution: 450 μm - 3000au, 850 μm - 4400au, $\text{NH}_3(1,1)$, $\text{NH}_3(2,2)$ - 1800 au



このフィラメント構造の性質を求める

Pineda et al. (2015)

● Results

- 細かい構造の検出

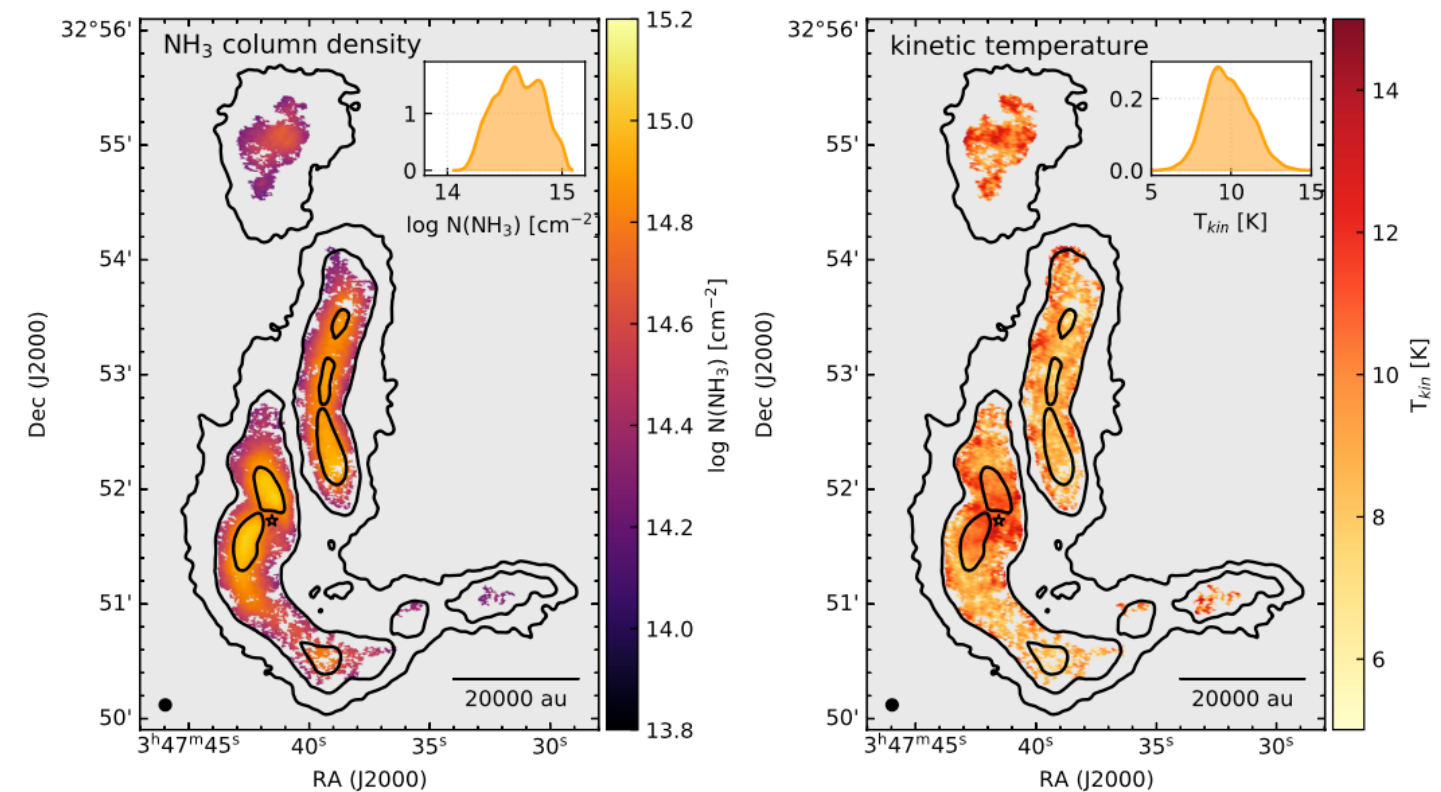
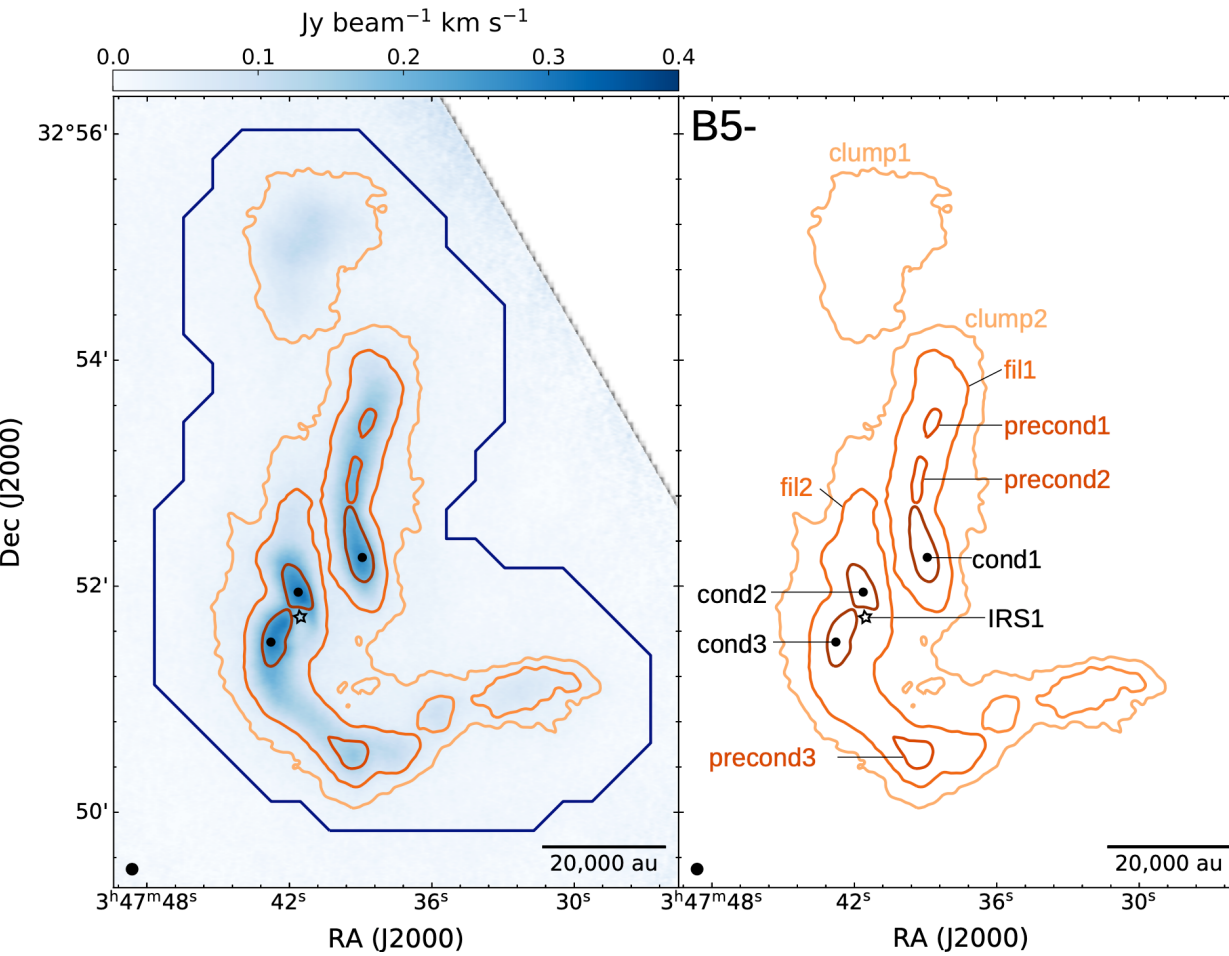
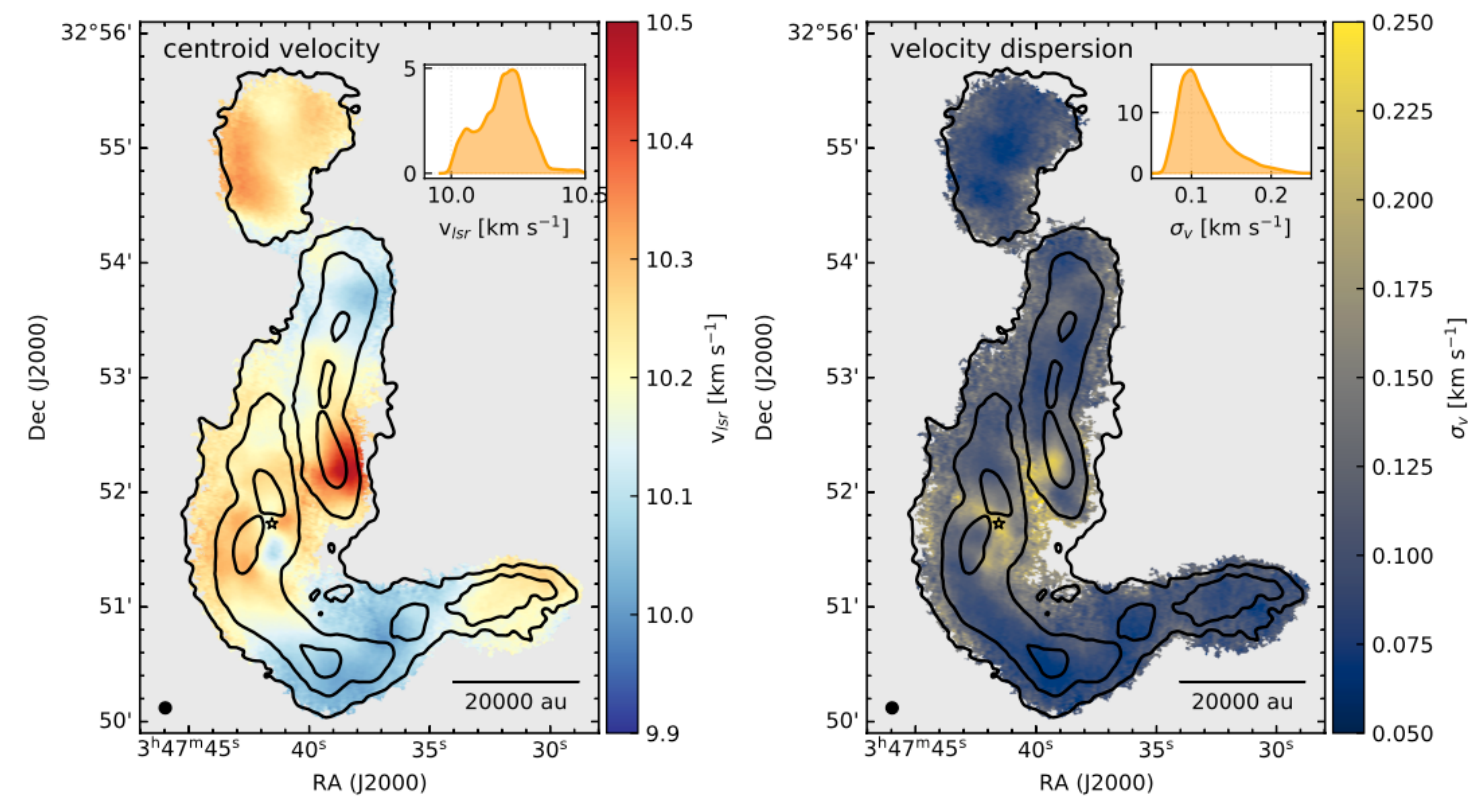


Table 1. Averaged properties of the substructure of the coherent region of B5, shown in Fig. 1.

ID	$\langle \log(N(\text{NH}_3)) \rangle$ [cm $^{-2}$]	$\langle T_{\text{kin}} \rangle$ [K]	$\langle v_{\text{lsr}} \rangle$ [km/s]	$\langle \sigma_{\text{nt}} \rangle$ [km/s]
[B5-]				
clump1	14.42 ± 0.12	10.7 ± 1.3	10.26 ± 0.05	0.06 ± 0.02
clump2	14.65 ± 0.20	9.7 ± 1.3	10.18 ± 0.09	0.09 ± 0.04
fil1	14.66 ± 0.18	9.2 ± 1.2	10.22 ± 0.11	0.10 ± 0.04
fil2	14.65 ± 0.19	9.9 ± 1.3	10.19 ± 0.09	0.09 ± 0.04
precond1	14.82 ± 0.03	8.4 ± 1.0	10.13 ± 0.01	0.08 ± 0.01
precond2	14.85 ± 0.02	8.5 ± 0.9	10.22 ± 0.01	0.08 ± 0.01
precond3	14.70 ± 0.05	8.3 ± 0.6	10.05 ± 0.03	0.04 ± 0.01
cond1	14.87 ± 0.05	8.6 ± 0.7	10.36 ± 0.08	0.14 ± 0.04
cond2	14.94 ± 0.06	10.8 ± 0.7	10.24 ± 0.03	0.12 ± 0.03
cond3	14.94 ± 0.06	10.6 ± 0.9	10.28 ± 0.03	0.11 ± 0.03



● Results

- フィラメント構造の性質

► Plummer function (model of cylindrical filament)

$$n(r) = \frac{n_0}{\left[1 + (r/R_{\text{flat}})^2\right]^{p/2}} + n_{\text{bkg}}$$

$$\rightarrow \Sigma(R) = A_p \frac{\Sigma_0}{\left[1 + (R/R_{\text{flat}})^2\right]^{\frac{p-1}{2}}} + \Sigma_{\text{bkg}},$$

where

$$\Sigma_0 = n_0 R_{\text{flat}}.$$

r : cylindrical radius

n_0 : central density of the cylinder

R : projected radius

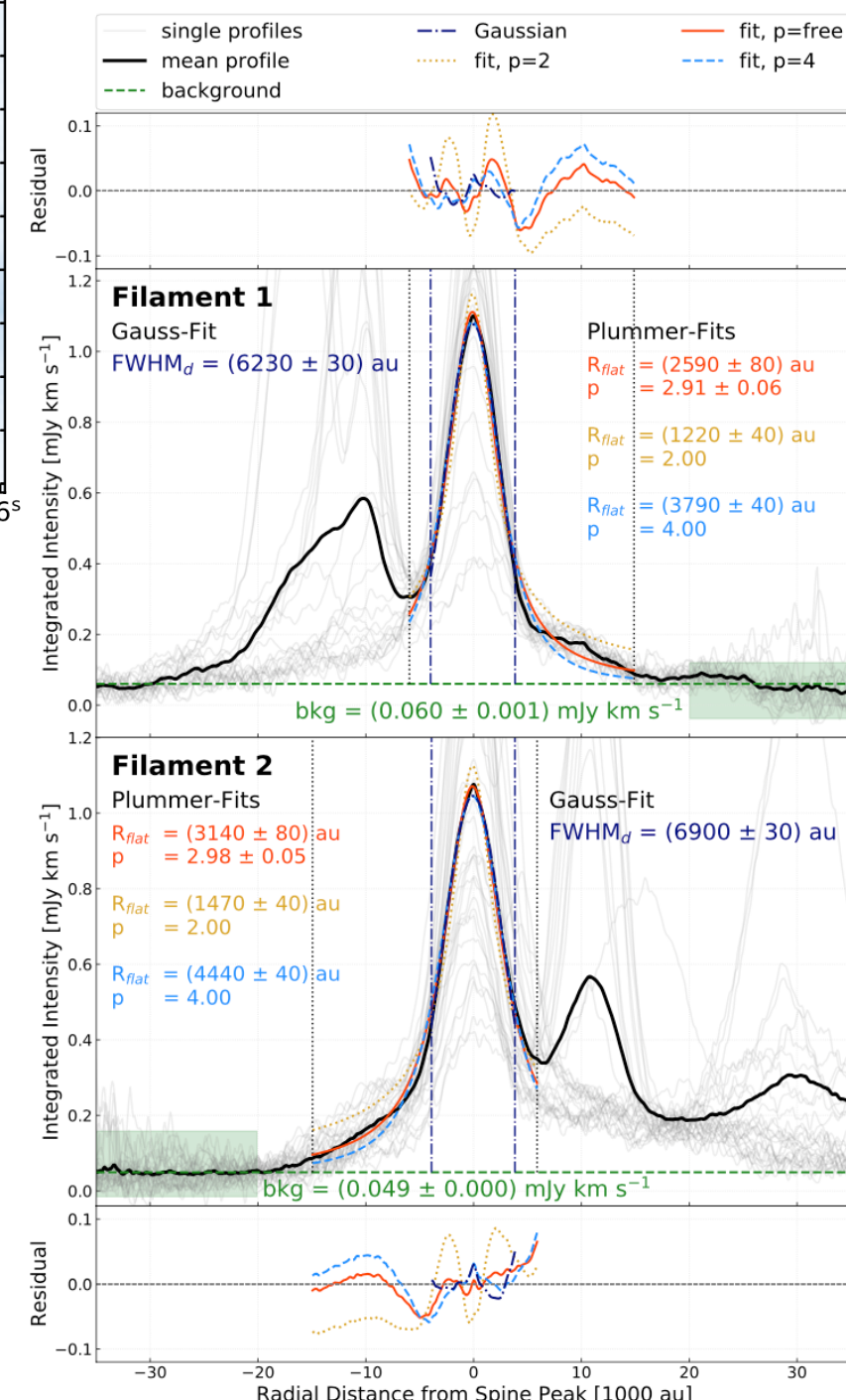
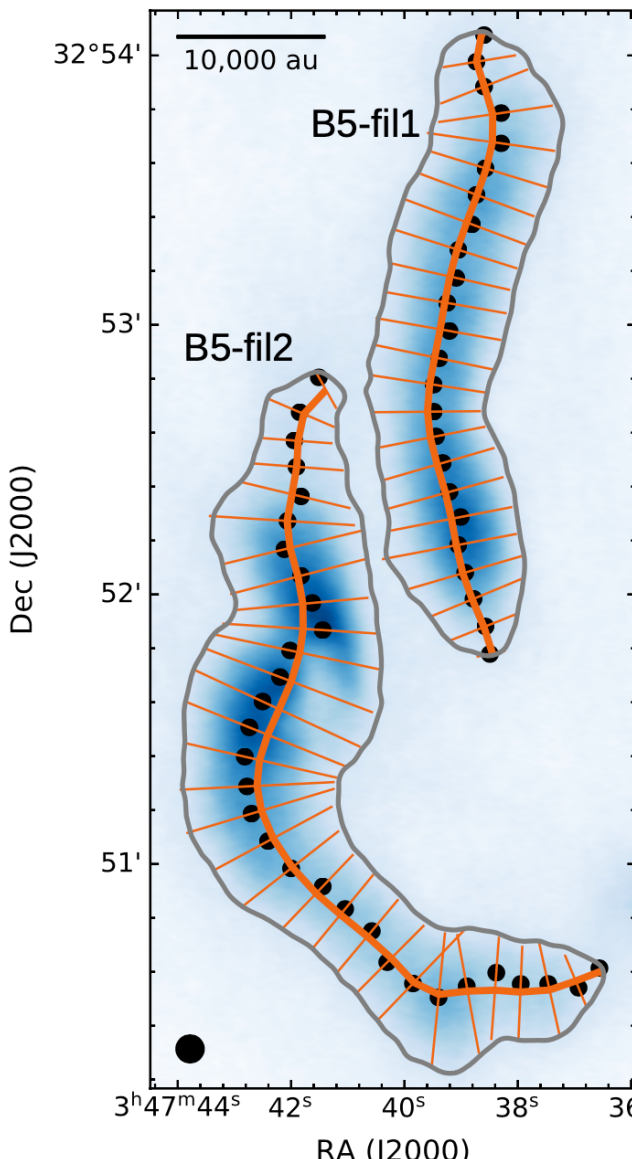
R_{flat} : radius of the flat inner section of the cylinder

A_p : finite constant factor

p : density profile power-low index

Σ_{bkg} : background surface density

n_{bkg} : background density



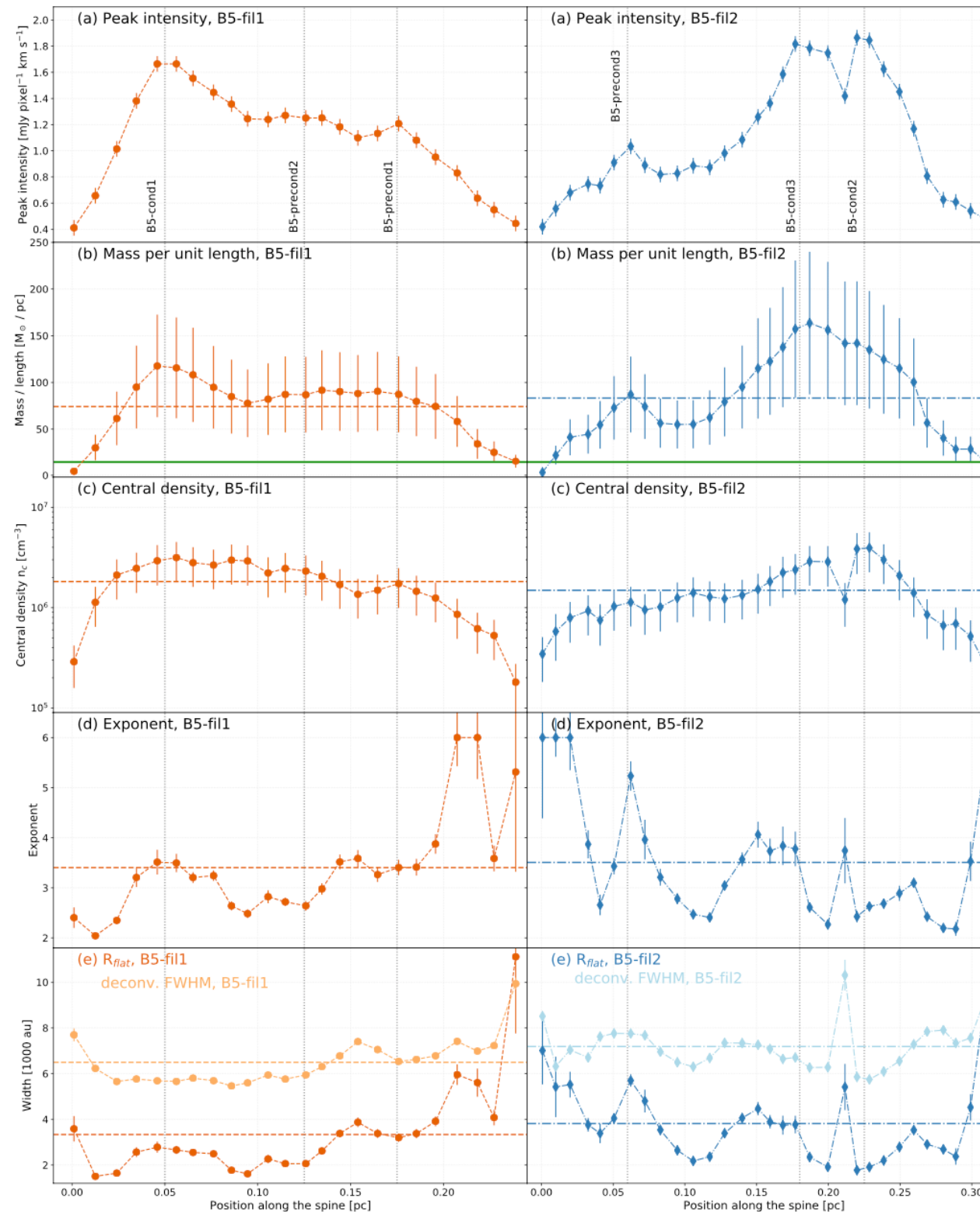
► Gaussian

$$g(R) = \frac{A_G}{\sigma_G \sqrt{2\pi}} \exp\left(-\frac{(R - \mu_G)^2}{2\sigma_G^2}\right) + g_{\text{bkg}},$$

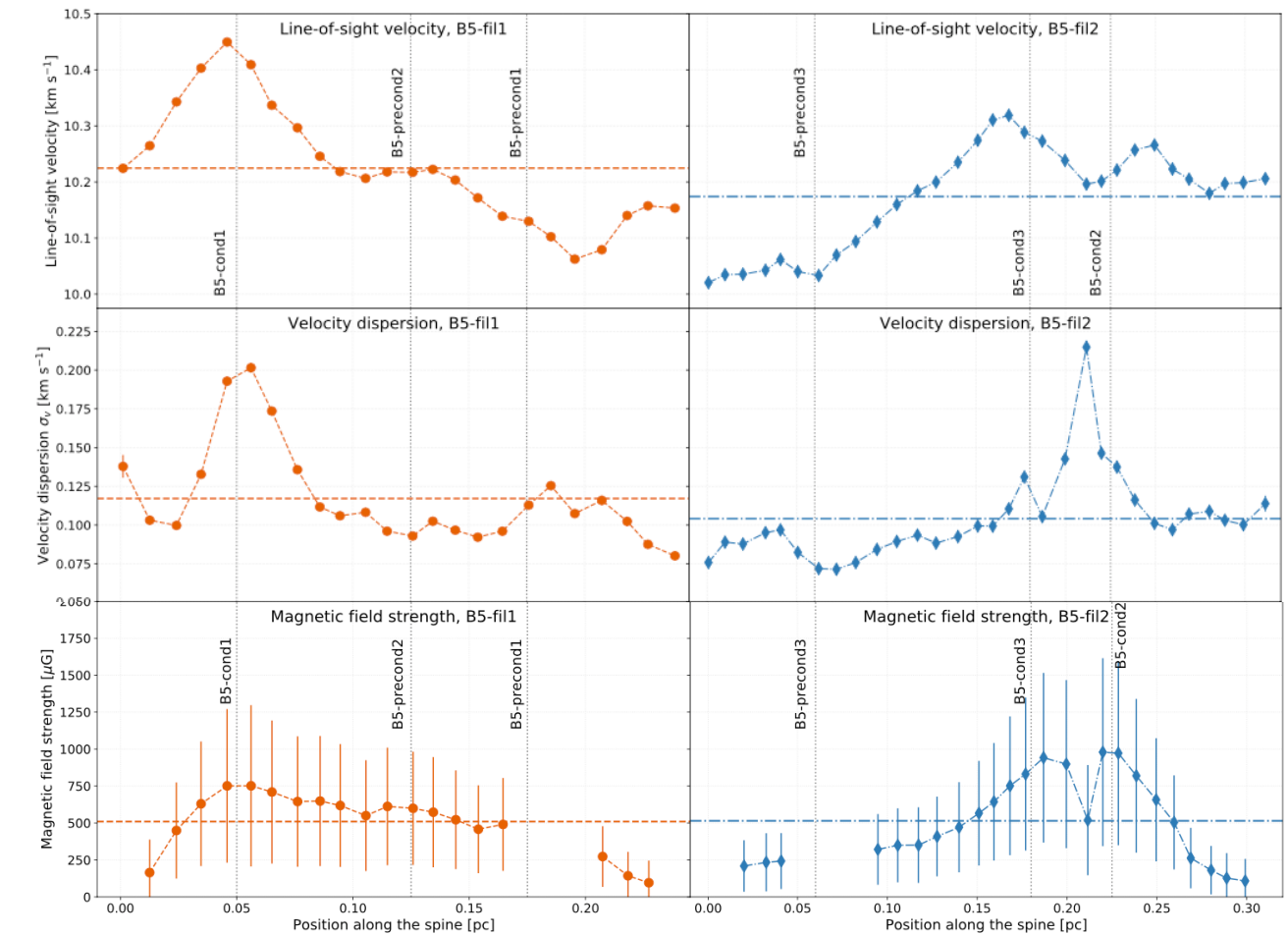
A_G : amplitude

σ_G : variance

μ_G : expected value

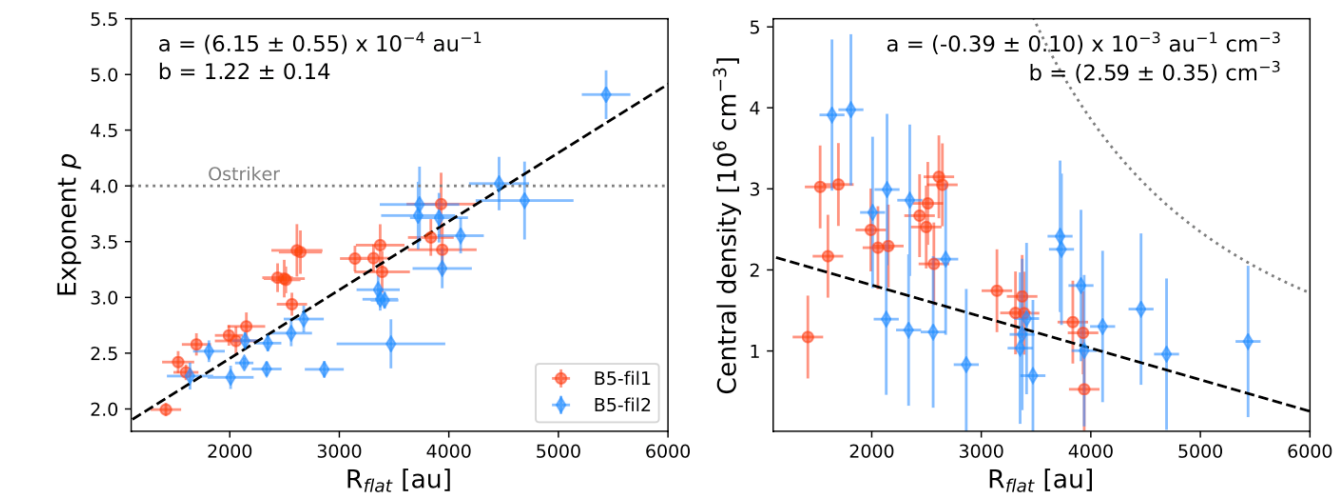


- ▶ $M/L \sim 80 M_{\odot} \text{pc}^{-1}$
(highly super-critical)
- ▶ $\text{FWHM} \sim 2 \times R_{\text{flat}}$



► $B_z \sim 500 \mu\text{G}$ (upper limit)

$$B_z = \sigma_v \sqrt{8\pi\mu_p m_H n_0 \left(\frac{(M/L)_{\text{obs}}}{(M/L)_{\text{crit,nt}}} - 1 \right)}.$$



► p と R_{flat} , Central density と R_{flat} に相関
が見られる

33. Outflows, envelopes, and disks as evolutionary indicators in Lupus YSOs

Vazzano et al.

<https://arxiv.org/pdf/2101.05330v1.pdf>

Prestellar ~ Protostellar の異なる進化段階の天体について、よく使用されている進化段階のトレーサー (T_{bol} , outflow...) の検証を行い、一貫性があるかどうか調べる

- Sample
 - Lupus complex に存在する7天体 (Prestellar - Protostellar)
 - ▶ SOLA(The Soul of Lupus with ALMA, Saito et al. 2015) を元に選出
(可視-cm波のデータによるSED fittingで進化段階を推定)
 - ▶ Protostellar candidate: Single source (non-multiple)
 - ▶ Prestellar candidate: density greater than critical density (not transient clumps)



同じ環境下 (interstellar radiation field, gas temperature, chemical composition)
かつ同じ観測設定 (beam size, distance, spatial resolution, sensitivity) のもとで
トレーサーの検証が可能

Table 1. Observed sources. (*): Classification from SOLA catalog (PC=Prestellar core, 0=Class 0, I=Class I, LI=Late-Class I).

Source name	Obs coordinates R.A,Dec(J2000)	Obs mode	Map size	Time on source (min)	Flux calibrator	Phase calibrator	Bandpass calibrator	Lupus cloud	Clasif.*
AzTEC-lup1-2	15:44:59, -34:17:07	Single-field	60"	2.0	J1427-4206	J1610-3958	J1427-4206	I	PC
AzTEC-lup3-5	16:09:00, -39:07:38	Single-field	60"	2.0	J1427-4206	J1610-3958	J1427-4206	III	PC
IRAS 15398-3359	15:43:02, -34:09:07	Mosaic	110"×90"	10.2	Ganymede	J1626-2951	J1517-2422	I	0
IRAS 16059-3857	16:09:18, -39:04:53	Mosaic	280"×110"	18.8	J1256-0547	J1610-3958	J1924-2914	III	0
Merin 28	16:24:51, -39:56:32	Mosaic	280"×110"	18.8	Callisto	J1610-3958	J1924-2914	VI	I
Sz 102	16:08:29, -39:03:11	Single-field	60"	2.0	J1427-4206	J1610-3958	J1427-4206	III	I
J160115-41523	16:01:16, -41:52:36	Mosaic	280"×110"	18.8	Ganymede	J1604-4441	J1337-1257	IV	LI

- Observation and Archive data (ALMA)

- SOLA observations
 - ALMA 7m array and TP (resolution $\sim 8''$: 1240 AU)
 - Band6 (1.3 mm continuum, $^{12}\text{CO}(2-1)$, $\text{SiO}(5-4)$, $\text{N}_2\text{D}^+(3-2)$, $\text{C}^{18}\text{O}(2-1)$)
- ALMA archive continuum data
 - Band 3, 6, 7, 8
- ALMA archive molecular data
 - Band 6 (12m, 7m, TP)

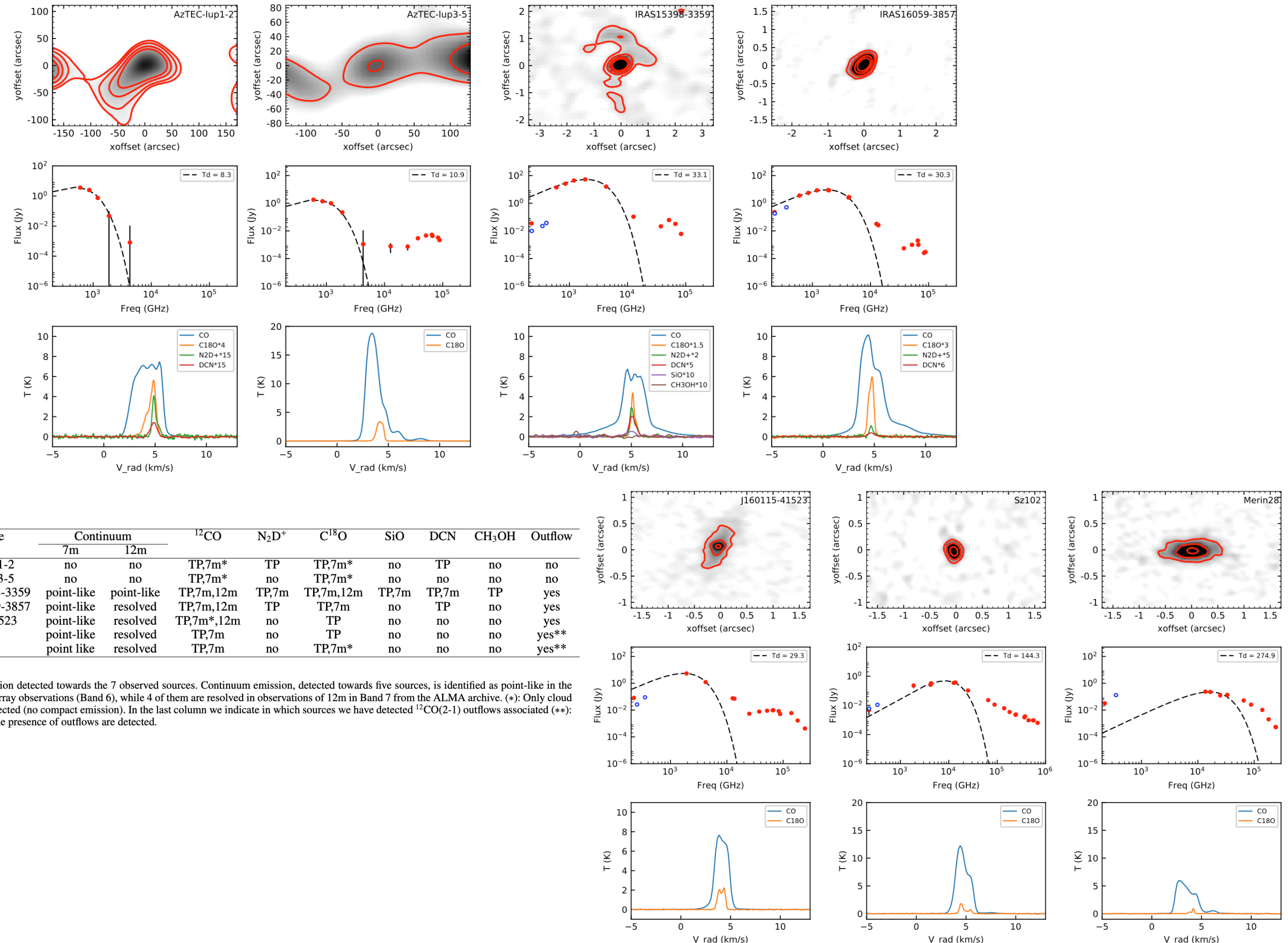
Table 2. Observational parameters of the high resolution continuum emission obtained from ALMA archive. Data described in Section 3.2

Project	Band	Ctl freq (GHz)	Resolution "×"	# Ant	B_{min} - B_{max} (m)	Time on source (seg)	Calibrator	Flux	Phase	Bandpass
IRAS 15398-3359										
2013.1.00879.S	6	225.646	0.44×0.41	32	19- 650	1229	Titan	J1534-3526	J1427-4206	
2011.0.00628.S	7	343.420	0.55×0.36	32	19-558	180	Titan	J1534-3526	J15427-406	
2013.1.00244.S	8	402.004	0.35×0.26	32	21-538	1511	Titan	J1517-2422	J1427-4206	
IRAS 16059-3857										
2015.1.00306.S	3	107.679	1.86×1.54	36	15-452	2104	J1517-2422	J1610-3958	J1517-2422	
2013.1.00879.S	6	225.645	0.45×0.40	32	19-650	1241	Titan	J1534-3526	J1427-4206	
2013.1.00474.S	7	357.981	0.25×0.14	32	15-1466	132	Ceres	J1610-3958	J1517-2422	
J160155-41523										
2016.1.00571.S	3	97.548	0.39×0.29	40	18-3143	241	J1427-4206	J1610-3958	J1517-2422	
2016.1.00459.S	6	254.706	0.20×0.14	40	16-2692	393	J1517-2422	J1610-3958	J1517-2422	
2013.1.00474.S	7	352.343	0.22×0.13	32	15- 1574	143	Ceres	J1610-3958	J1517-2422	
Sz102										
2016.1.01239.S	6	225.282	0.24×0.18	40	16-2647	180	J1427-4206	J1610-3958	J1517-2422	
2016.1.01239.S	7	335.141	0.19×0.18	40	15-1124	270	J1517-2422	J1610-3958	J1517-2422	
Merin 28										
2013.1.00474.S	7	352.343	0.19×0.13	32	15-1574	132	Ceres	J1610-3958	J1517-2422	

Table 3. Observational parameters of the e high resolution ALMA archive's molecular data. Data described in Section 3.3

Project	Band	Resolution "×"	# Ant	B_{min} - B_{max} (m)	Obs time (min)	Calibrator	Flux	Phase	Bandpass
IRAS 15398-3359									
2013.1.00879.S	6	0.57×0.49	34-36	20-650	88	Titan	J1534-3526	J1427-4206	
IRAS 16059-3857									
2017.1.00019.S	6	1.73×1.10	48-50	15-360	84.6	J1517-2422	J1610-3958	J1517-2422	
J160155-41523									
2015.1.01510.S	6	0.92×0.85	43	15-453	16	J1617-5848	J1604-4228	J1427-420	

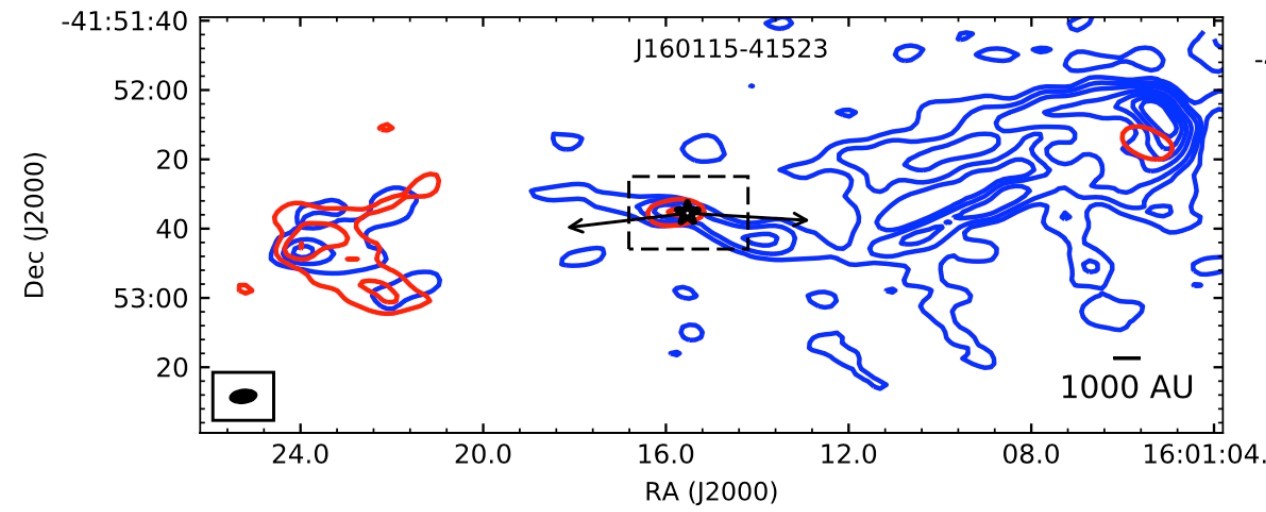
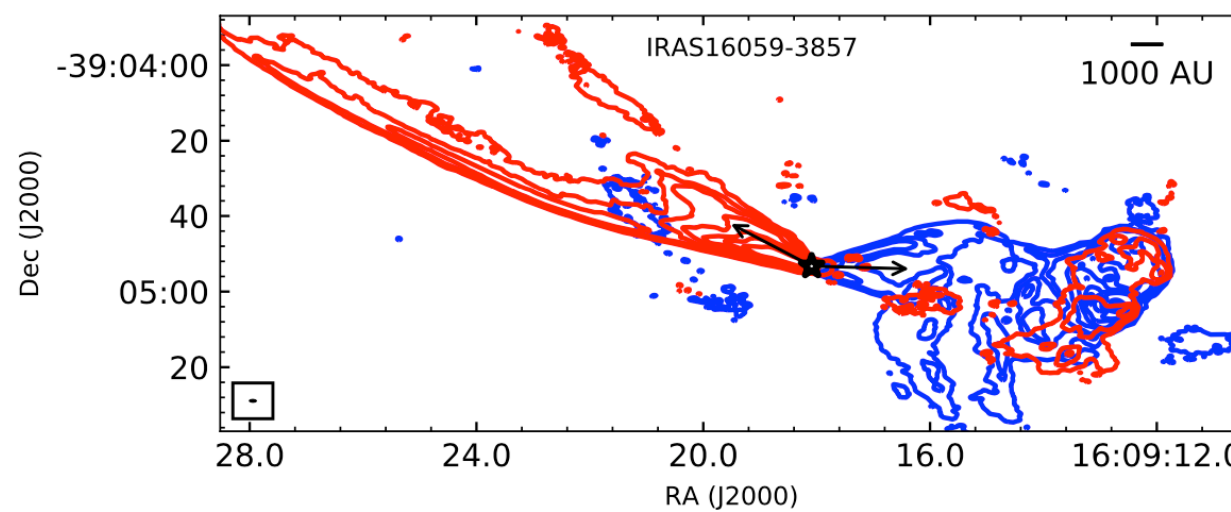
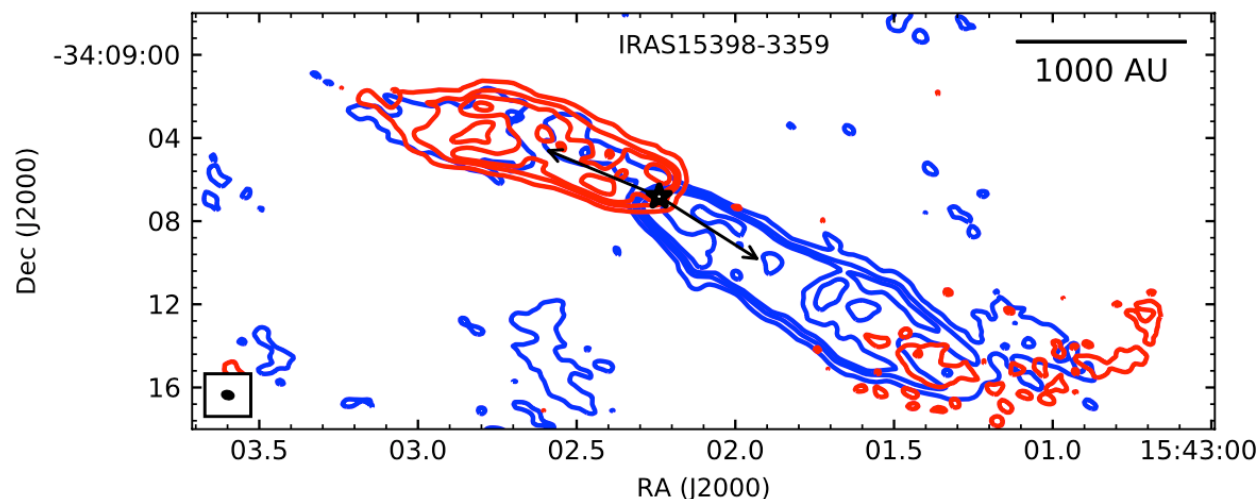
● Results



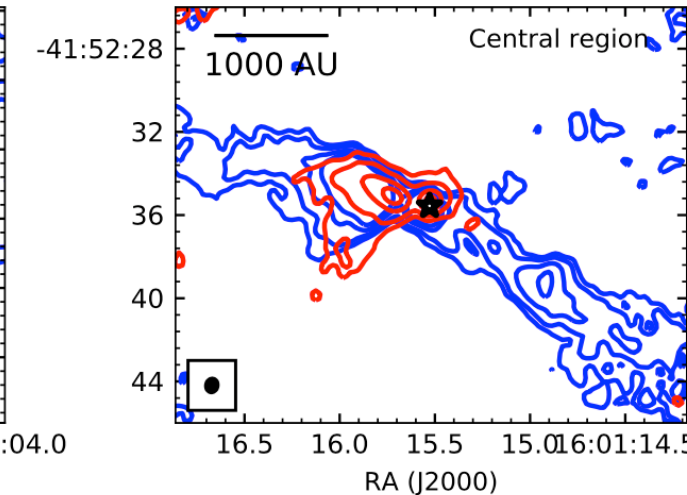
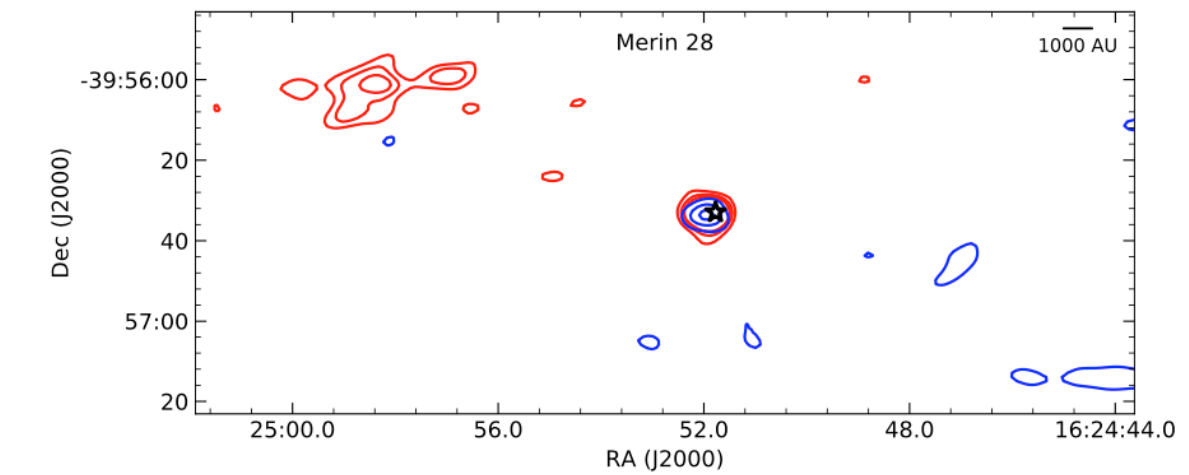
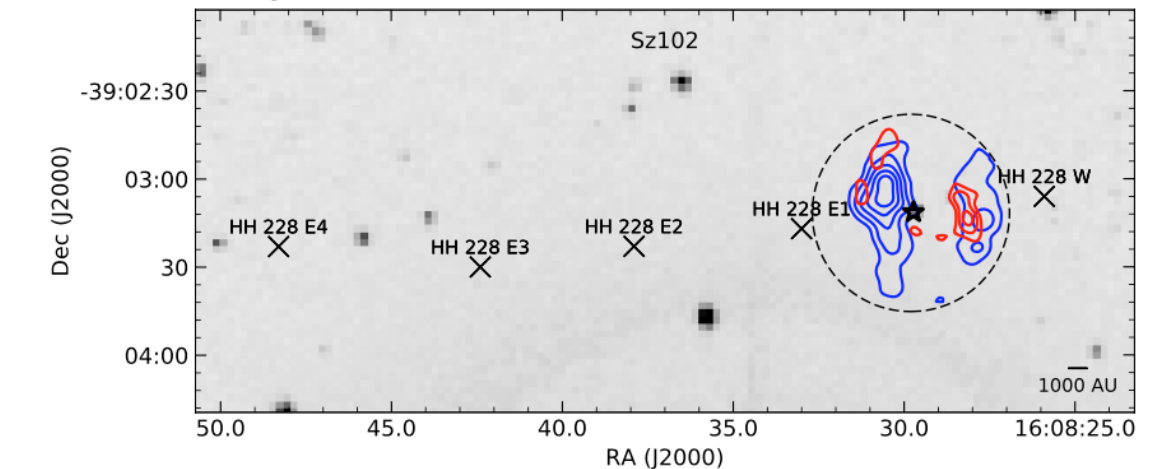
- Results

- Outflow structures

Cleary detected outflows



Signs of the presence of outflow



● Results

- 進化段階の検証
 - ▶ SED (T_{bol} , L_{bol}/L_{submm} , M_{disk}/M_{env} , spectral index α , β)
 - ✓ T_{bol} , L_{bol}/L_{submm} , M_{disk}/M_{env} は 進化段階をトレース (特にProtostellarのClass) しているようだが、完全ではなく同じような進化段階にある天体に関してはその詳細を調べるのは難しい
 - ✓ Spectral index α (IR), β (millimeter)は今回の天体に関しては使えなかった
 - ▶ Chemical evolution (N_2D^+ , DCN, N_2H^+ , HCN, CO, CH_3OH , SO, SiO)
 - ✓ DCN, N_2D^+ が検出された天体は若い、 CH_3OH , SO, SiOは若いアウトフローをトレースしている可能性がある、などと判断できるが、Shock chemistryを考慮すると複雑になり、注意が必要
 - ▶ Outflow evolution (opening angle, velocity extent, momentum, energy, mass-loss rate, momentum flux...)
 - ✓ Outflowの特徴だけで進化段階を区別するのは難しい (これまで示唆されていた、opening angleが進化とともに大きくなる、長さは短くなる、等の傾向は確認されなかった。
 - ✓ ただし、今回のサンプルではenergyやmomentum fluxと年齢に相関が見られた

Source	SED	T_{bol}	Chemistry	Outflow	Overall
AzTEC-lup1-2	pre-stellar	early class 0	pre-stellar/early class 0	none	pre-stellar
AzTEC-lup3-5	pre-stellar(*)	early class 0(*)	only CO envelope	none	pre-stellar
IRAS 16059-3857	early class 0	early class 0	pre-stellar/early class 0	early class 0	early class 0
IRAS 15398-3359	late class 0	late class 0/early class I	early class 0	class 0	class 0
J160115-41523	late class 0	late class 0/early class I	only CO disk	late class 0	late class 0
Sz 102	class I	class I	only CO disk	weak detection	class I
Merin 28	class I	class I	only CO disk	weak detection	class I

Table 13. Summary of the evolutionary classifications obtained for each source according to the different indicators. (*) We consider that only the FIR bump is associated with AzTEC-lup3-5.

27. Constraining Protoplanetary Disk Accretion and Young Planets Using ALMA Kinematic Observations

Rabago et al.

<https://arxiv.org/pdf/2102.03007v2.pdf>

ABSTRACT

Recent ALMA molecular line observations have revealed 3-D gas velocity structure in protoplanetary disks, shedding light on mechanisms of disk accretion and structure formation. 1) By carrying out viscous simulations, we confirm that the disk's velocity structure differs dramatically using vertical stress profiles from different accretion mechanisms. Thus, kinematic observations tracing flows at different disk heights can potentially distinguish different accretion mechanisms. On the other hand, the disk surface density evolution is mostly determined by the vertically integrated stress. The sharp disk outer edge constrained by recent kinematic observations can be caused by a radially varying α in the disk. 2) We also study kinematic signatures of a young planet by carrying out 3-D planet-disk simulations. The relationship between the planet mass and the "kink" velocity is derived, showing a linear relationship with little dependence on disk viscosity, but some dependence on disk height when the planet is massive (e.g. $10M_J$). We predict the "kink" velocities for the potential planets in DSHARP disks. At the gap edge, the azimuthally-averaged velocities at different disk heights deviate from the Keplerian velocity at similar amplitudes, and its relationship with the planet mass is consistent with that in 2-D simulations. After removing the planet, the azimuthally-averaged velocity barely changes within the viscous timescale, and thus the azimuthally-averaged velocity structure at the gap edge is due to the gap itself and not directly caused to the planet. Combining both axisymmetric kinematic observations and the residual "kink" velocity is needed to probe young planets in protoplanetary disks.

Key words: accretion – accretion disks – astroparticle physics - dynamo - magneto-hydrodynamics (MHD) - instabilities - turbulence

ALMAの観測が1)降着メカニズムと2)惑星の性質の解明にどのように活用できるか検証

- 円盤の速度構造は異なる降着メカニズムによる垂直方向の応力分布によって大きく変化する
→ 速度構造から降着メカニズムを識別可能？
- 円盤のギャップの端で見られ方位角方向に平均化された速度構造は、惑星ではなくギャップ自体に起因するもの → 円盤内の惑星探査には軸対象の運動学的観測と"キンク"速度両方必要

28. Accretion and outflow activity in proto-brown dwarfs

Riaz et al.

<https://arxiv.org/pdf/2012.08612.pdf>

ABSTRACT

We present a near-infrared study of accretion and outflow activity in 6 Class 0/I proto-brown dwarfs (proto-BDs) using VLT/SINFONI spectroscopy and spectro-imaging observations. The spectra show emission in several [Fe II] and H₂ lines associated with jet/outflow activity, and in the accretion diagnostics of Pa β and Br γ lines. The peak velocities of the [Fe II] lines ($>100 \text{ km s}^{-1}$) are higher than the H₂ lines. The Class 0 proto-BDs show strong emission in the H₂ lines but the [Fe II] lines are undetected, while the Class I objects show emission in both [Fe II] and H₂ lines, suggesting an evolutionary trend in the jets from a molecular to an ionic composition. Extended emission with knots is seen in the [Fe II] and H₂ spectro-images for 3 proto-BDs, while the rest show compact morphologies with a peak on-source. The accretion rates for the proto-BDs span the range of $(2 \times 10^{-6} - 2 \times 10^{-8}) M_{\odot} \text{ yr}^{-1}$, while the mass loss rates are in the range of $(4 \times 10^{-8} - 5 \times 10^{-9}) M_{\odot} \text{ yr}^{-1}$. These rates are within the range measured for low-mass protostars and higher than Class II brown dwarfs. We find a similar range in the jet efficiency for proto-BDs as measured in protostars. We have performed a study of the Brackett decrement from the Br 7-19 lines detected in the proto-BDs. The upper Brackett lines of Br 13–19 are only detected in the earlier stage systems. The ratios of the different Brackett lines with respect to the Br γ line intensity are consistent with the ratios expected from Case B recombination.

Key words:

brown dwarfs – stars: jets – stars: winds, outflows – ISM: individual objects: Mayrit 1701117 – ISM: individual objects: HH 1165 – ISM: individual objects: MHO 2156 – ISM: individual objects: MHO 3256 – ISM: individual objects: MHO 3257

近赤外の分光-撮像観測でproto-BDのaccretionとoutflow活動を調べた

- Class 0-BDではH₂は検出されるが[FeII]は検出されない。Class I-BDでは両方検出される
→ ジェットの組成が分子組成からイオン組成に変わっていくことを示唆
- 全てのproto-BDがoutflow構造を持つ
→ 角運動量の保存のため、進化の初期段階でoutflowが重要であることを示唆

29. GASTON: Galactic Star Formation with NIKA2. Evidence for the mass growth of star-forming clumps

GASTON collaboration, Rigby et al.

<https://arxiv.org/pdf/2101.08811v2.pdf>

ABSTRACT

Determining the mechanism by which high-mass stars are formed is essential for our understanding of the energy budget and chemical evolution of galaxies. By using the New IRAM KIDs Array 2 (NIKA2) camera on the Institut de Radio Astronomie Millimétrique (IRAM) 30-m telescope, we have conducted high-sensitivity and large-scale mapping of a fraction of the Galactic plane in order to search for signatures of the transition between the high- and low-mass star-forming modes. Here, we present the first results from the Galactic Star Formation with NIKA2 (GASTON) project, a Large Programme at the IRAM 30-m telescope which is mapping $\approx 2 \text{ deg}^2$ of the inner Galactic plane (GP), centred on $\ell = 23^\circ 9, b = 0^\circ 05$, as well as targets in Taurus and Ophiuchus in 1.15 and 2.00 mm continuum wavebands. In this paper we present the first of the GASTON GP data taken, and present initial science results. We conduct an extraction of structures from the 1.15 mm maps using a dendrogram analysis and, by comparison to the compact source catalogues from *Herschel* survey data, we identify a population of 321 previously-undetected clumps. Approximately 80 per cent of these new clumps are 70 μm -quiet, and may be considered as starless candidates. We find that this new population of clumps are less massive and cooler, on average, than clumps that have already been identified. Further, by classifying the full sample of clumps based upon their infrared-bright fraction – an indicator of evolutionary stage – we find evidence for clump mass growth, supporting models of clump-fed high-mass star formation.

Key words: Galaxy: disc – stars: formation – stars: massive – ISM: evolution – ISM: structure – surveys

IRAM30mのNIKA2カメラを用いた大規模サーベイ (1.15, 2.00mm) のfirst results

- Hershelでは検出されていなかった、新たな321個のクランプを発見
(その80%はstarless clumpと考えられる、また既存のものより低温で低質量)
- 全サンプルを赤外線の明るさの割合（進化段階の指標）に沿って分類した結果、clumpの質量は進化と共に増加する傾向を発見
→ “clump-fed high-mass star formation”モデルを示唆

30. C¹⁸O, ¹³CO, and ¹²CO abundances and excitation temperature in the Orion B molecular cloud: An analysis of the precision achievable when modeling spectral line within the Local Thermodynamic Equilibrium approximation

Roueff et al.

<https://arxiv.org/pdf/2005.08317v1.pdf>

ABSTRACT

Context. CO isotopologue transitions are routinely observed in molecular clouds to probe the column density of the gas, the elemental ratios of carbon and oxygen, and to trace the kinematics of the environment.

Aims. We aim at estimating the abundances, excitation temperatures, velocity field and velocity dispersions of the three main CO isotopologues towards a subset of the Orion B molecular cloud, which includes IC 434, NGC 2023, and the Horsehead pillar.

Methods. We use the Cramer Rao Bound (CRB) technique to analyze and estimate the precision of the physical parameters in the framework of local-thermodynamic-equilibrium (LTE) excitation and radiative transfer with an additive white Gaussian noise. We propose a maximum likelihood estimator to infer the physical conditions from the 1–0 and 2–1 transitions of CO isotopologues. Simulations show that this estimator is unbiased and efficient for a common range of excitation temperatures and column densities ($T_{\text{ex}} > 6 \text{ K}$, $N > 10^{14} - 10^{15} \text{ cm}^{-2}$).

Results. Contrary to the general assumptions, the different CO isotopologues have distinct excitation temperatures, and the line intensity ratios between different isotopologues do not accurately reflect the column density ratios. We find mean fractional abundances that are consistent with previous determinations towards other molecular clouds. However, significant local deviations are inferred, not only in regions exposed to UV radiation field but also in shielded regions. These deviations result from the competition between selective photodissociation, chemical fractionation, and depletion on grain surfaces. We observe that the velocity dispersion of the C¹⁸O emission is 10% smaller than that of ¹³CO. The substantial gain resulting from the simultaneous analysis of two different rotational transitions of the same species is rigorously quantified.

Conclusions. The CRB technique is a promising avenue for analyzing the estimation of physical parameters from the fit of spectral lines. Future work will generalize its application to non-LTE excitation and radiative transfer methods.

Key words. ISM: molecules; ISM: clouds; Radiative transfer; Methods: data analysis, Methods: statistics

Orion B molecular cloudにおいてC¹⁸O, ¹³CO, ¹²COの性質をCRB法を用いて調べた

- 異なる同位体は異なる励起温度を持ち、同位体比は柱密度比を反映していない
- UVにさらされていない領域 (shielded region) でもアバンダנסに変化がある

32. High-accuracy estimation of magnetic field strength in the interstellar medium from dust polarization

Skalidis and Tassis

<https://arxiv.org/pdf/2010.15141v2.pdf>

ABSTRACT

Context. A large-scale magnetic field permeates our Galaxy and is involved in a variety of astrophysical processes such as star formation and cosmic ray propagation. Dust polarization has been proven one of the most powerful observables for studying the field properties in the interstellar medium (ISM). However, it does not provide a direct measurement of its strength. Different methods have been developed which employ both polarization and spectroscopic data in order to infer the field strength. The most widely applied method has been developed by [Davis \(1951\)](#) and [Chandrasekhar & Fermi \(1953\)](#) (DCF). The DCF method relies on the assumption that isotropic turbulent motions initiate the propagation of Alfvén waves. Observations, however, indicate that turbulence in the ISM is anisotropic and non-Alfvénic (compressible) modes may be important.

Aims. Our goal is to develop a new method for estimating the field strength in the ISM, which includes the compressible modes and does not contradict the anisotropic properties of turbulence.

Methods. We adopt the following assumptions: 1) gas is perfectly attached to the field lines; 2) field line perturbations propagate in the form of small-amplitude MHD waves; 3) turbulent kinetic energy is equal to the fluctuating magnetic energy. We use simple energetics arguments that take into account the compressible modes to estimate the strength of the magnetic field.

Results. We derive the following equation: $B_0 = \sqrt{2\pi\rho\delta v} / \sqrt{\delta\theta}$, where ρ is the gas density, δv is the rms velocity as derived from the spread of emission lines, and $\delta\theta$ is the dispersion of polarization angles. We produce synthetic observations from 3D MHD simulations and we assess the accuracy of our method by comparing the true field strength with the estimates derived from our equation. We find a mean relative deviation of 17%. The accuracy of our method does not depend on the turbulence properties of the simulated model. In contrast DCF, even when it is combined with the [Hildebrand et al. \(2009\)](#) and [Houde et al. \(2009\)](#) method, systematically overestimates the field strength.

Conclusions. Compressible modes can affect significantly the accuracy of methods that are based solely on Alfvénic modes. The formula that we propose includes compressible modes; however it is applicable only in regions with no self-gravity. Density inhomogeneities may bias our estimates to lower values.

Key words. magnetic field – interstellar medium (ISM) – dust polarization

ISMにおける新たな磁場強度の測定方法の確立

- 新しい手法は既存のもの(DCF)よりも誤差が低く、乱流の性質にも依存しない
↑ただし、自己重力でない系でしか使えず、密度が不均一な場合は推定値が低く見積もられる可能性がある？